Exploring the Accuracy and Reliability of Plasma Fluid Models for Direct Current Glow Discharges

Thomas Underwood
University of Florida, Gainesville, FL, USA

A. V. Khrabrov, I. D. Kaganovich
Princeton Plasma Physics Laboratory, Princeton, NJ, USA
(Dated: August 17, 2012)

Glow discharges are of fundamental importance to a variety of industrial applications such as plasma processing, discharge lighting and plasma chemistry. Therefore, a detailed understanding of the physical phenomena that occur within glow discharges is necessary for further advances in design and optimization of relevant plasma applications. Of the various plasma modeling approaches, most use either a fluid approximation, kinetic (particle) approach, or a hybrid extended fluid model. Although each method has its own set of unique advantages, recent advances in hybrid techniques have shown unique promise to maintain computational efficiency and accuracy. The validity of assumptions within the fluid and hybrid models will be established by direct comparison with results obtained using an electrostatic direct implicit particle-in-cell code (EDIPIC). The accuracy of these assumptions will also be explored within each region of a typical glow discharge and relevant theory will be discussed to explain these results.

INTRODUCTION

As plasma glow discharges impact so many industrial applications, it is important to understand both the differences in existing modeling techniques and why they exist. Historically, plasma glow discharges were simulated using either a kinetic approach emphasizing fidelity or a fluid model emphasizing numerical efficiency. More recent advances have aimed at reformulating the fluid model to include additional kinetic effects such as non-local ionization and variable electron transport coefficients.

It has long been known that classical plasma fluid models are inaccurate within regions of low electric field strength. Typically in such models the ionization rate is assumed to have an exponential dependence on the local E/p. This inherently limits the accuracy of the model as it allows ionization only to occur within the cathode fall where large values of E/p exist. However, within such regions as the negative glow and Faraday dark space where the electric field is comparatively weak, little to no ionization is predicted. Experimental observations have been shown to contradict this as the negative glow and Faraday dark space are both highly luminous. This luminosity indicates both non-local ionization and excitation from fast electrons emitted from the cathode [1].

In order to correct the inaccuracies caused by the local-field approximation (LFA) of the ionization frequency, hybrid extended fluid models have been developed. Such models [2, 3], incorporate non-local ionization effects by solving the Boltzmann equation for the electron transport coefficients as a function of the electron temperature, T_e. As the variable electron temperature is explicitly used to determine ionization rates throughout a plasma discharge, this model is frequently called the local-mean-energy approximation (LMEA). The electron temperature is then solved using the conservation of energy balance equation which accounts for energy transfer by heat conduction in the form of Joule heating as well as volume processes in the form of elastic and inelastic scattering.

In this work, two independent fluid models are presented based on an upwind finite-differencing scheme to better understand the physical differences between the LFA and LMEA models. In addition, both are compared directly with a electrostatic direct implicit particle-in-cell code (EDIPIC) to better characterize inaccuracies still present within each model [4]. Finally, the electron and ion fluxes produced from the EDIPIC results will be decomposed into drift and diffusive components using particle averaging techniques and compared with the fluid models.

MODEL

In this section an overview of the models employed in this paper will be provided. In addition, the boundary conditions and numerical schemes used to produce the relevant results will be provided.

Local-Field Approximation

The gas-discharge fluid model is based on the drift-diffusion approximation of the conservation of momentum balance equation. Using this approximation, the species continuity equations for both electrons and ions

can be given as,

$$\frac{\partial n_{i,e}}{\partial t} + \nabla \cdot \mathbf{\Gamma}_{i,e} = S_{i,e}, \tag{1}$$

where $\mathbf{\Gamma}$ is the species flux,

$$\mathbf{\Gamma}_{i,e} = \pm \mu_{i,e} n_{i,e} \mathbf{E} - D_{i,e} \nabla n_{i,e}, \tag{2}$$

S is the net ionization rate and μ and D are the species mobility and diffusion constants respectively. The equation system is completed by using the electrostatic approximation to determine both the electric potential, ϕ, and electric field, $\mathbf{E}$, as a function of position,

$$\nabla^2 \phi = -e \left(\frac{n_i - n_e}{\epsilon_0} \right), \tag{3}$$

$$\mathbf{E} = -\nabla \phi. \tag{4}$$

Transport Coefficients

Within this model a constant electron and ion temperature of 1 eV and 300 K respectively is assumed. The Einstein relation,

$$D = \frac{k_b T}{e} \mu, \tag{5}$$

is assumed for both electron and ions to determine a relationship between diffusion and mobility. Table I provides the exact values for argon discharges.

Source Term

The net ionization rate within Eq. 1 assumes an exponential dependence on the strength of the electric field,

$$\alpha = Ap \exp\left(\frac{-Bp}{\|\mathbf{E}\|} \right), \tag{6}$$

where α is Townsend's coefficient and A and B are empirical values that take on values of 12 $\text{cm}^{-1}\text{Torr}^{-1}$ and 180 $\text{Vcm}^{-1}\text{Torr}^{-1}$ [1] respectively for argon gas. Using Eq. 6, the net ionization rate can be written as,

$$S_{i,e} = \alpha \|\mathbf{\Gamma}_e\|. \tag{7}$$

TABLE I: Electron and ion transport coefficients used for the LFA fluid model. All constants are in cgs units while p is evaluated in Torr.

Coefficient	Value	Source
μ_e	$3.6 \times 10^5 p^{-1}$	[5]
μ_i	$1.6 \times 760 p^{-1}$	[6]
D_i	$0.048 \times 760 p^{-1}$	[6]
D_e	$3.6 \times 10^5 p^{-1}$	[5]

Local Mean-Energy Approximation

The hybrid fluid model expands upon the those that rely on the LFA by incorporating an additional equation governing energy transfer for electrons,

$$\frac{\partial n_\epsilon}{\partial t} + \nabla \cdot \mathbf{\Gamma}_\epsilon = -e \mathbf{\Gamma}_e \cdot \mathbf{E} - \frac{3}{2} n_e \nu_{ea} k_b \left(T_e - T_i \right) - \sum_j \Delta E_j R_j, \tag{8}$$

where $\bar{\epsilon} = 3/2 k_b T_e$ is the mean energy and $n_\epsilon = n_e \bar{\epsilon}$ is the mean energy density. Γ_ϵ is mean the energy flux,

$$\Gamma_\epsilon = \mu_\epsilon n_\epsilon \mathbf{E} - D_\epsilon \nabla n_\epsilon, \tag{9}$$

while μ_ϵ and D_ϵ are electron energy transport coefficients.

Within the source of energy transfer in Eq. 8, the first term involving the electron flux governs energy transfered to electrons via Joule heating. The second and third terms govern elastic and inelastic scattering events for electrons. Within Eq. 8, ν_{ea} refers to the total collision frequency between electrons and neutral atoms while R_j refers to the rate coefficients for the j^{th} inelastic collisional process.

Table II details the air chemistry model used within this paper. It incorporates a total of three elementary reactions in argon gas. This can be extended to a total of seven reactions if a metastable atom continuity equation is also solved, such as in Ref [2].

Transport Coefficients

To obtain variable electron transport coefficients, a steady-state Boltzmann equation solver [7] was used to evaluate

$$\mu_e = -\frac{\gamma}{3 n_\infty} \int_0^\infty \frac{\epsilon}{\tilde{\sigma}_m} \frac{\partial F_0}{\partial \epsilon} d\epsilon, \tag{10}$$

$$D_e = \frac{\gamma}{3 n_\infty} \int_0^\infty \frac{\epsilon}{\tilde{\sigma}_m} F_0 d\epsilon, \tag{11}$$

as a function of the mean electron energy determined by Eq. 8. Within Eq. 10, n_∞ is the background number density, $\gamma = (2e/m)^{1/2}$ is a constant and F_0 is the isotropic portion of the electron energy distribution function. Electron energy transport coefficients are calculated by using the approximate relationship of,

$$\mu_\epsilon = \frac{5}{3} \mu_e, \tag{12}$$

$$D_\epsilon = \frac{5}{3} D_e. \tag{13}$$

Ion transport coefficients are assumed constant and obtained directly from Table I. One could also evaluate this as a semi-empirical function of the electric field although little experimental variation has been shown over the electric field strengths considered in this study [6].

TABLE II: Air chemistry reactions considered in this paper. All rate coefficients were calculated using a Boltzmann solver [7].

Index	Reaction	Type	ΔE (eV)	Rate
1	$e + Ar \rightarrow e + Ar$	Elastic Collision	0	Boltz.
2	$e + Ar \rightarrow e + Ar^+$	Direct Ionization	15.8	Boltz.
3	$e + Ar \leftrightarrow e + Ar^*$	Excitation	11.5	Boltz.

Source Term

The ionization source in the hybrid model uses rate coefficients for each of the reactions included in the air chemistry model. The electron and ion source rate can thus be given by,

$$S_{i,e} = R_2 n_\infty n_e, \tag{14}$$

where the source rate for both electron and ions are equal due to conservation of charge.

Boundary Conditions

At both the cathode and anode, the ion flux was specified to be [2],

$$\widehat{\mathbf{n}} \cdot \mathbf{\Gamma_i} = 1/4 \nu_i n_i + \alpha n_i \mu_i \left(\widehat{\mathbf{n}} \cdot \mathbf{E}\right), \tag{15}$$

where $\nu_j = \sqrt{8 k_b T_j / \pi m_j}$ is the thermal velocity of species j, $\widehat{\mathbf{n}}$ is the unit vector pointing toward the wall and α is a switching function of the form,

$$\alpha = \begin{cases} 1 & \text{if } \widehat{\mathbf{n}} \cdot \mathbf{E} > 0 \\ 0 & \text{if } \widehat{\mathbf{n}} \cdot \mathbf{E} < 0 \end{cases} \tag{16}$$

The electron flux and mean energy flux boundary conditions were selected such that the electron flux would be at an absolute maximum under steady-state conditions at the anode and a minimum at the cathode. With that in mind, at the cathode the electron flux and mean energy flux were constrained to,

$$\widehat{\mathbf{n}} \cdot \mathbf{\Gamma}_e = 1/4 \nu_e n_e - \gamma \left(\widehat{\mathbf{n}} \cdot \mathbf{\Gamma}_i\right), \tag{17}$$

$$\widehat{\mathbf{n}} \cdot \mathbf{\Gamma}_\epsilon = 1/3 v_e n_\epsilon - 2 k_b T_e \gamma \left(\widehat{\mathbf{n}} \cdot \mathbf{\Gamma}_i\right). \tag{18}$$

while at the anode,

$$\Gamma_e = 1/4 \nu_e n_e, \tag{19}$$

$$\Gamma_\epsilon = 1/4 \nu_\epsilon n_\epsilon, \tag{20}$$

where γ is the secondary emission coefficient present at the cathode.

Numerical Scheme

The governing fluid equations for both models that have been presented involve considerable numerical challenges. They are together a system of coupled nonlinear equations.

Implicit Method

The LFA fluid model was solved using a fully coupled implicit finite-difference scheme. Such an implicit scheme offers significant advantages over explicit schemes in that the Courant-Friedrichs-Lewy (CFL) condition,

$$\frac{\nu_d \Delta t}{\Delta x} \leq 1, \tag{21}$$

need not be satisfied. This allows for a larger numerical time-step which is essential for efficiency.

Using second-order central differencing, Eq. 1 written for electrons becomes,

$$\left(\frac{n_{\kappa,i}^{n+1} - n_{\kappa,i}^{n}}{\Delta t}\right) + \left(\frac{\Gamma_{\kappa,i+1/2}^{n+1} - \Gamma_{\kappa,i-1/2}^{n+1}}{\Delta x}\right) = \alpha_i^{n+1} \| \Gamma_{e,i}^{n+1} \|. \tag{22}$$

Here subscripts i and κ refer to grid spacing and charge species respectively while n refers to discretization in time. The species flux is evaluated on a staggered mesh with respect to the independent variables to improve numerical stability. In addition, to damp artificial numerical oscillations that are prevalent in nonlinear convective-diffusion problems, a Sharfetter-Gummel discretization scheme [8] is assumed. This form, written as,

$$\Gamma_{\kappa,i+1/2}^{n+1} = b_{\kappa,i+1/2}^{n+1} \eta, \tag{23}$$

$$\eta = \left[\frac{(D_\kappa n_\kappa)_i^{n+1}}{1 - \exp\left(-\Delta x b_{\kappa,i+1/2}^{n+1}\right)} + \frac{(D_\kappa n_\kappa)_{i+1}^{n+1}}{1 - \exp\left(\Delta x b_{\kappa,i+1/2}^{n+1}\right)}\right], \tag{24}$$

is a form of upwind differencing that simplifies to a pure diffusive flux in the limit of low electric field strength and a drift flux in the limit of low diffusion. In Eq. 23, $b_{\kappa,i} = (\mu_\alpha E / D_\alpha)_i$.

Poisson's equation is also evaluated using a second-order central differencing scheme for improved accuracy. It can be written as,

$$\frac{\phi_{i+1} - 2\phi_i + \phi_{i-1}}{\Delta x^2} = -e \left(\frac{n_i - n_e}{\epsilon_0}\right)_i. \tag{25}$$

Semi-Implicit Method

The local mean-energy fluid model involves two additional numerical difficulties. First, numerical look-up

tables must be generated from Boltzmann solvers featuring transport and rate coefficients as a function of mean electron energy. In addition, the electron energy equation must also be solved in a coupled fashion to the previously developed equations.

These additions make a fully implicit scheme even more computationally difficult. To improve numerical efficiency, a semi-implicit scheme was introduced for this model to decouple Eq. 3 by expanding $\rho^{n+1} \approx \rho^n + \Delta t \frac{\partial \rho}{\partial t}$. Using this form of the updated net charge density, Poisson's Eq. becomes,

$$\nabla^2 \phi^{n+1} \approx -\frac{1}{\epsilon_0} \left[n_i^n - n_e^n + \Delta t \left(\nabla \cdot \mathbf{\Gamma}_e^n - \nabla \cdot \mathbf{\Gamma}_i^n \right) \right], \quad (26)$$

where the revised Poisson's equation now includes a projected contribution from drift and diffusive fluxes on the electric potential at the next time step.

The electron energy equation was discretized in the same manner as Eq. 23 and was decoupled from the species continuity equations by using the electron transport coefficients in Eqs. 1-14 from the previous time-step. Numerical look-up tables were generated as a function of electron temperature using BOLSIG+ [7].

Particle-In-Cell Code

The particle-in-cell (PIC) code used throughout this work for comparison is described in Ref. 4. To better model anisotropy, a scattering algorithm described in Ref. 9 was used. Using the first Born approximation in quantum mechanics, the normalized differential scattering cross section used in the PIC code becomes,

$$I(\epsilon, \chi) = \frac{1}{4\pi} \frac{1 + 8\epsilon}{(1 + 4\epsilon - 4\epsilon \cos \chi)^2}. \quad (27)$$

The probability and scattering angle respectively were obtained from Eq. 27 and can be given as,

$$P(\epsilon, \chi) = \frac{(1 + 8\epsilon) \sin^2\left(\frac{\chi}{2}\right)}{1 + 8\epsilon \sin^2\left(\frac{\chi}{2}\right)}, \quad (28)$$

$$\cos \chi = 1 - \frac{2R}{1 + 8\epsilon (1 - R)}, \quad (29)$$

where R is a uniformily distributed random number from 0 to 1 and $\epsilon = E/E_0$ is the dimensionless energy of electrons. E_0 was found to be approximately 22 eV based on a curve fit of the ratio between the total and momentum transfer cross-sections.

Electron drift and diffusion coefficients were also calculated directly from the particle data in the PIC code using Eqs. 12-13. To better understand the effect anisotropic fast electrons play in electron flux, such electrons were ignored in calculating the electron transport coefficients. Using particle averaging techniques, Eqs. 12-13 were evaluated in the form,

$$\mu_e = -\frac{\gamma}{3n_\infty} \frac{\sum_j \Delta N_j \epsilon_j^{-1/2} \frac{d}{d\epsilon} \left[\frac{\epsilon_j}{\tilde{\sigma}_{m,j}} \right]}{\sum_j \Delta N_j}, \quad (30)$$

$$D_e = \frac{\gamma}{3n_\infty} \frac{\sum_j \Delta N_j \epsilon_j^{1/2} \tilde{\sigma}_{m,j}^{-1}}{\sum_j \Delta N_j}, \quad (31)$$

where both coefficients were discretized in both real and phase space for evaluation of the kinetic integrals.

RESULTS

To better understand any differences that exist between the three plasma models considered in this paper, two cases were analyzed in argon gas. As summarized in Table III, the background gas pressure, electrode separation distance and secondary electron emission coefficient were all held constant between the cases. Voltage was varied parametrically between the cases to better characterize its effect on the accuracy within fluid models.

Case 1

In simulation of a 250 Volt glow discharge in argon gas at 1 Torr, significant deviation was observed between the three plasma models considered. According to experimental observations made by [10], the parameters for case 1 highlighted in Table III represent the experimental transition between a stable and unstable glow discharge. A secondary electron emission coefficient of 0.06 was selected based on measured electron yields from various clean metal surfaces for incident Ar and Ar^+ ion beams.

As shown in Fig. 1 , the hybrid fluid model predicted a stable discharge on the microsecond timescale. In that figure, $x^* = x/L$ is the normalized position relative to the total discharge length L and $t^* = t/T$ is the normalized time relative to the time taken to reach steady-state, T. To resolve this discharge with the hybrid model, a total of 250 equally spaced nodes were used to properly resolve transient gradients that develop as the ionization rate peak drifts from the anode to the cathode. A constant time-step on the order of 10^{-10} seconds was used.

TABLE III: Simulation parameters used for the results included in this paper.

Case	Voltage [V]	L [cm]	Pressure [Torr]	γ
1	250	1	1	0.06
2	600	1	1	0.06

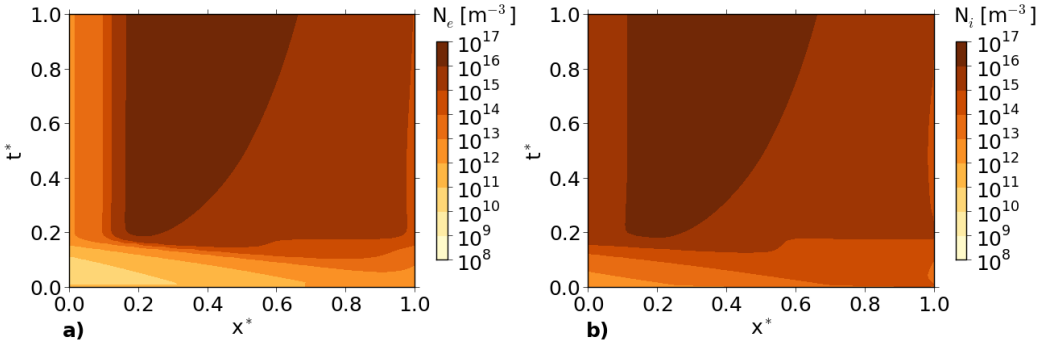

FIG. 1: Normalized spatial and temporal evolution for a) N_e and b) N_i using the hybrid fluid model.

Additional tests were run with smaller time-steps on the order of Maxwell's characteristic time to test the accuracy of the semi-implicit approach. Negligible changes in transient or steady-state profiles were obtained using these time-steps.

Fig. 1 also shows that the cathode sheath is resolved in approximately 20% of the time taken to resolve the bulk quasineutral region. This is consistent with expectations for both the kinetic and fluid models. In both models this occurs because of the high electric field strengths and mobilities experienced by electrons close to the cathode. Such strong forces cause an equilibrium to be achieved on a much faster timescale than in the bulk where electric field strengths are comparatively weak.

The spatial and temporal development of the cathode fall layer can also be seen in Fig. 2. In Fig. 2, the cathode fall layer can be seen extending a couple of millimeters where large gradients in the electric potential are shown. Similarly, a steady-state electron temperature profile is reached that shows a peak near the cathode with mean temperatures near 50 eV followed by a sharp gradient leading into the quasineutral bulk.

Both the LFA fluid code and kinetic particle code do not predict a steady discharge for the first set of parameters included in Table III. As shown in Fig. 3, the LFA fluid model significantly under-predicts bulk electron and

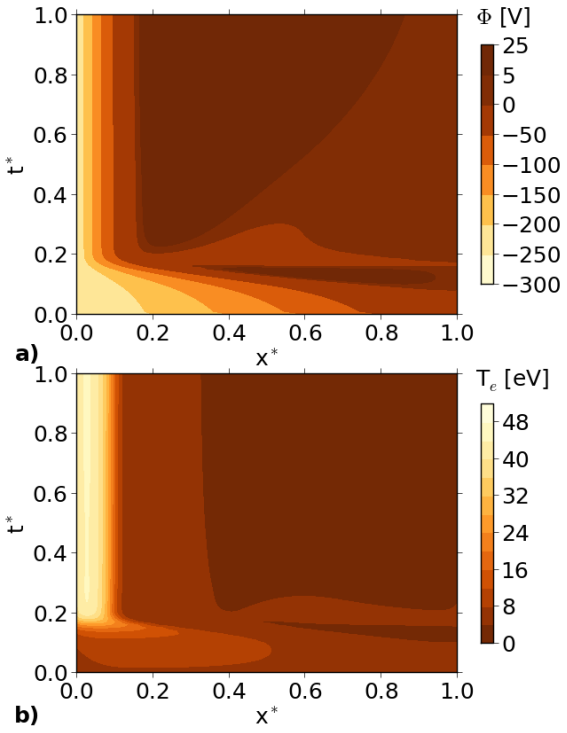

FIG. 2: Normalized spatial and temporal evolution for a) ϕ and b) T_e using the hybrid fluid model.

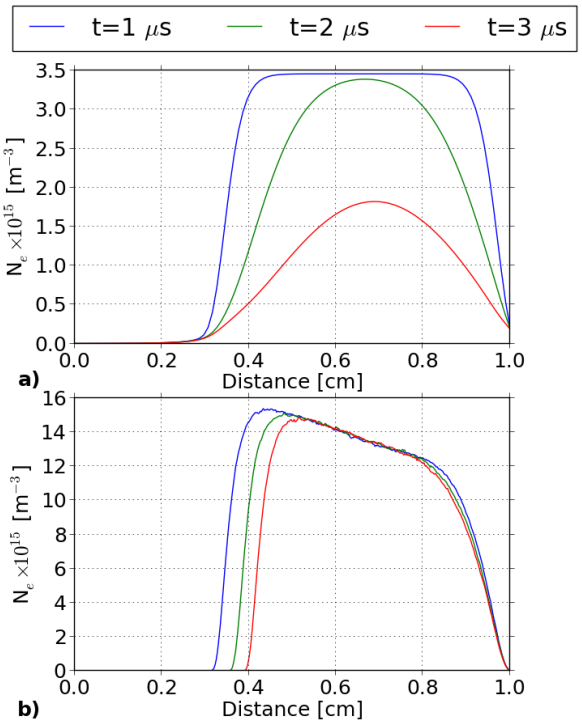

FIG. 3: Temporal evolution for N_e at a variety of time-steps for the a) local-field approximation and b) kinetic models.

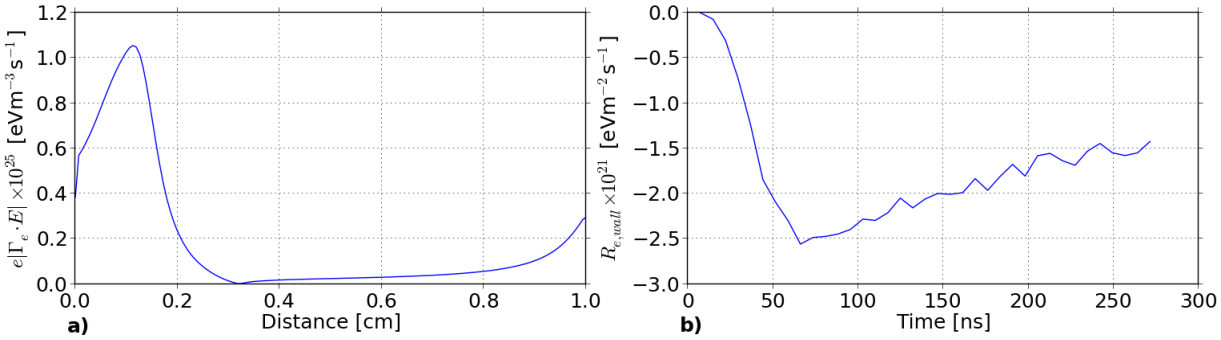

FIG. 4: Normalized spatial and temporal evolution for a) N_e and b) N_i using the hybrid fluid model.

ion number densities compared to both the kinetic and hybrid models. As the discharge progresses it has insufficient ionization in the bulk to replenish losses through the electrodes and thus a discharge is not sustained. Such a result is not entirely unexpected for the LFA fluid model because its ionization source approaches zero in the limit of a vanishing electric field. The particle-in-cell code also predicts a vanishing discharge in Fig. 3. However, unlike with the LFA fluid model, the PIC code predicts a stable bulk number density. The discharge is then slowly consumed as the cathode sheath grows in space.

To better understand why the hybrid fluid model seems to differ from the particle-in-cell result, it is necessary to investigate the role that fast anistropic electrons play in the discharge. Such electrons are not explicitly accounted for in either the LFA or hybrid fluid models as a Maxwellian velocity distribution is inherently assumed. Fig. 4 shows a comparison of the power lost from the discharge from fast (> 30 eV) electrons compared directly with Joule heating over the length of the discharge. The relative importance of fast electron energy loss can be shown by integrating the contribution from Joule heating over the length of the discharge to obtain a a value of $\sim 10^{22}$ [eVm^{-2}s^{-1}]. As this mode of energy loss is not included in Eq. 8, it could help to explain why the hybrid fluid model seems to over-predict ionization and and in the case of 250 Volts, predicts a stable discharge. The excess energy left in the system by not modeling fast electrons will lead to higher source rate coefficients and therefore higher ionization.

Case 2

In simulation of a 600 Volt glow discharge in argon at 1 Torr, closer agreement was obtained between the three plasma models considered. Geometric and gas properties detailed in Table III were kept constant from case 1 to case 2 while voltage was increased to better understand its comparative impact on both the fluid and kinetic models. By doing so, the agreement between the three models improved as all three models predicted a steady discharge on the microsecond timescale, shown in Fig. 5.

Although all three models converge to a steady discharge, the local-field approximation based fluid model still predicts significantly different physics for both ions and electrons. Much like the 250 Volt case, it underpredicts the bulk electron and ion number density by an order of magnitude. The reason behind this is shown by the source rate spatial and temporal profiles in Fig. 6. This shows that the LFA fluid model underpredicts ionization in the bulk by a few orders of magnitude. When this is combined with the isothermal underprediction of both mobility and diffusion transport coef-

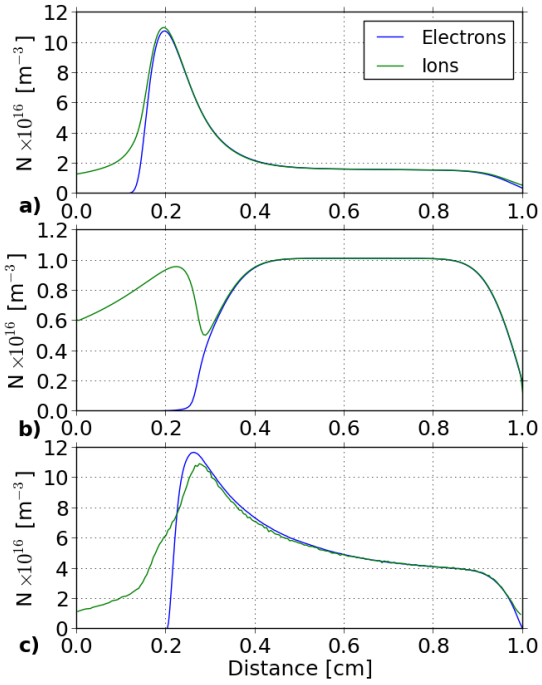

FIG. 5: Approximate steady-state spatial evolution of N_e for the a) hybrid b) LFA and c) kinetic (particle) models.

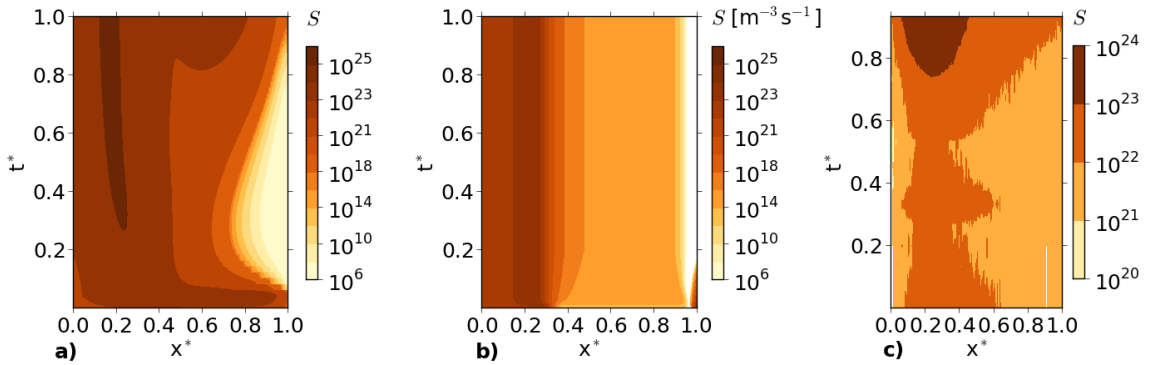

FIG. 6: Normalized spatial and temporal evolution of the ionization source rate for the a) hybrid b) LFA and c) kinetic (particle) models.

ficients present within the LFA model, the result is an order-of-magnitude inaccuracy in the steady-state solution.

The local-field approximation based fluid model also predicts a flat profile in the bulk of the discharge for 600 Volts compared to curved profiles for the other models, as shown in Fig. 6. This can be explained by inspecting the ionization rate profiles in time and space in Fig. 6. Unlike both the hybrid and kinetic models, the LFA model features a uniform ionization rate over the bulk region. In a region where ambipolar diffusion dominates, a uniform ionization rate along with isothermally determined electron transport coefficients will cause such a flat profile to exist. For the other two models considered in this work, peaks in the quasineutral region coincide with the position of absolute maximum ionization.

Fluxes

Fluxes were compared for the parameters detailed in case 2 of Table III. As shown in Fig. 7, significant deviation was obtained between the different models for the total electron and ion fluxes. Within the kinetic (particle) model, the electron and ion fluxes were calculated by counting the number of particles per unit area and time. This complete model of the species flux makes no assumptions regarding the form of the particle distribution function. For both fluid models considered in this paper (and all that assume a drift-diffusion form), the current is decomposed into two separate terms: one responsible for drift motion and the other for diffusion. This approximation inherently assumes the distribution of electrons within a plasma as is weakly anisotropic.

Upon further inspection of Fig. 7, significant deviation in species current is predicted between the hybrid model and kinetic (particle) models. Even though the hybrid model produced similar profiles for electric potential and species number densities, it severely over-predicts the PIC results for flux. This over-prediction can be explained by examining the steady-state ($t^* = 1$) results from Fig. 6. As the hybrid fluid model approaches steady-state, the ionization rate close to the anode increases significantly. This increase is responsible for the larger steady-state flux as the integral of the ionization rate over space is equal to the flux. The LFA fluid makes a similar two-term approximation but under-predicts ionization so far in the bulk that any apparent inaccuracy is balanced out.

To better determine the role of fast electrons in approximation of electron flux, Eqs. 30-31 were used to approximate the drift and diffusion coefficients for the kinetic PIC code while ignoring electrons with energies above 30

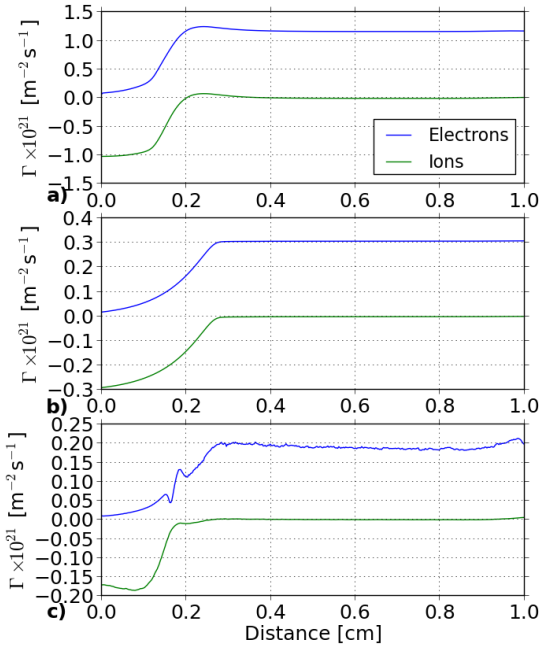

FIG. 7: Spatially varying electron and ion fluxes for 600 Volts using the a) hybrid b) LFA and c) kinetic (particle) models.

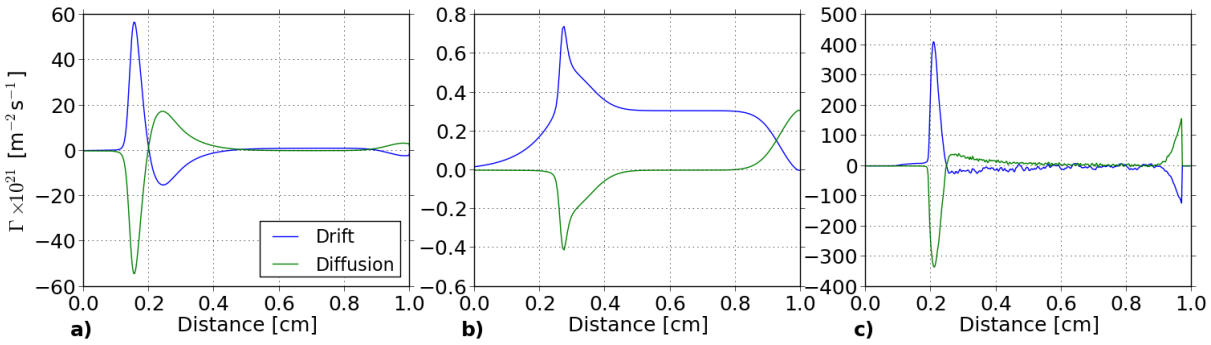

FIG. 8: Spatially varying drift and diffusive fluxes for 600 Volts using the a) hybrid b) LFA and c) kinetic (particle) models.

eV in the discharge. Using those results and taking a two term approximation of the particle distribution function, drift and diffusive fluxes were constructed. The results of this approximation is shown in Fig . 8 along with the results from the fluid models. When comparing the results from the two-term approximation of anisotropy with the total flux predicted by the PIC code, significant deviation is shown. It is also important to note that the drift and diffusive fluxes for the hybrid and PIC code feature similar profiles. Thus when variable transport coefficients are used, results in this work suggest that the effect of fast electrons causes significant prediction error for the species fluxes and plasma current.

CONCLUSION

In this work, the accuracy of the various plasma fluid models was evaluated for argon glow discharges. It was found that the hybrid fluid model significantly improved results in regions of low electric field strength within a glow discharge. In addition, it was found that the hybrid fluid model predicts the formation of a steady discharge over a wider range of parameters. This was likely because the governing energy equation does not include fast electron loss to the walls. Such emission was found to be a significant fraction of the dominant mode of energy transfer for electrons at lower voltages. Finally, it was determined that the common two-term approximation of anisotropic distributions prevalent in drift-diffusion based fluid models leads to inaccuracy in prediction of current when variable electron and ion transport coefficients are used. Future work will focus on understanding the effects that gases with large mean-free-paths such as helium have on the accuracy of fluid models. In addition, work will be done to include more kinetic effects within such fluid models. An example of this would be to decompose the electron species into two separate balanced quantities. One for isotropically distributed electrons and another for fast emitted electrons.

ACKNOWLEDGEMENTS

The author wishes to thank Dr. Alex Khrabrov and Dr. Igor Kaganovich for the support and assistance they provided throughout the project. The author also wishes to thank the Department of Energy and Princeton Plasma Physics Laboratory for offering exceptional research opportunities such as the National Undergraduate Fellowship.

[1] Yu. P. Raizer, Gas Discharge Physics. Springer, Berlin, (1991).
[2] I. Rafatov et. al, Phys. Plasmas 19 (2012).
[3] M. M. Becker et. al, Com. Physics Commun. 180 (2009).
[4] Dmytro Sydorenko, (2006). Particle-in-Cell Simulations of Electron Dynamics in Low Pressure Discharges with Magnetic Fields. Ph.D. Thesis. University of Saskatchewan: Canada.
[5] J. F. Boeuf and L. C. Pitchford, Phys. Rev. E. 51 (1995) 137.
[6] Boris M. Smirnov, Reference Data on Atomic Physics and Atomic Processes. Spring, Berlin, (2008).
[7] G. M. Hagelaar et. al, Plasma Sources Sci. Technol. 14 (2005) 722-733.
[8] D. Scharfetter, H. Gummel, IEEE Trans. Elec. Dev. 16 (1969) 64.
[9] A. Okhrimovskyy et. al, Phys. Review E. 65 (2002).
[10] A. Phelps et. al, Plasma Sources Sci. Technol. 8 (1999) R21.